J|A|C|S
ARTICLES
Published on Web 05/23/2007

Beyond Exciton Theory: A Time-Dependent DFT and Franck−Condon Study of Perylene Diimide and Its Chromophoric Dimer

Aurora E. Clark,* Changyong Qin, and Alexander D. Q. Li

Contribution from the Department of Chemistry, Washington State University, Pullman, Washington 99164

Received December 7, 2006; E-mail: auclark@wsu.edu

Abstract: The diimide perylene motif exhibits a dramatic intensity reversal between the 0 → 0 and 0 → 1 vibronic bands upon $\pi-\pi$ stacking; this distinct spectral property has previously been used to measure folding dynamics in covalently bound oligomers and synthetic biological hybrid foldamers. It is also used as a tool to assess organization of the π-stacking, indicating the presence of H- or J-aggregation. The zeroth-order exciton model, often used to describe the optical properties of chromophoric aggregates, is solely a transition dipole coupling scheme, which ignores the explicit electronic structure of the system as well as vibrational coupling to the electronic transition. We have therefore examined the optical properties of gas-phase perylene tetracarboxylic diimide (PTCDI) and its chromophoric dimer as a function of conformation to relate the excited-state distributions predicted by exciton theory with that of time-dependent density functional theory (TDDFT). Using ground- and excited-state geometries, the Franck−Condon (FC) factors for the lowest energy molecular nature electronic transition have been calculated and the origin of the intensity reversal of 0 → 0 and 0 → 1 vibronic bands has been proposed.

Introduction

The diimide perylene motif has generated great interest because of its potential utilities in nanoscale field-effect transistors, light-harvesting solar cells, and robust organic dyes that are resistant to photobleaching.[1−10] One fascinating feature of the perylene motif is the dramatic intensity reversal between the 0 → 0 and 0 → 1 vibronic bands upon $\pi-\pi$ stacking; this distinct spectral property has been used to measure folding dynamics in covalently bound oligomers and synthetic biological hybrid foldamers.[11] Until recently, there have been few systematic and well-controlled studies of the influence of aggregate size and geometry upon the optical spectra. Previous work in solution has primarily involved concentration-dependent UV−vis spectroscopy, while thin-film research has examined the optical behavior as a function of thin-film depth. Both approaches have uncertainty in the interactions and in the order at the molecular level, which has prompted one of us (A.D.L.) to examine the absorption and fluorescence of well-defined covalently bound perylene diimide oligomers.[12−14] Both linear, foldable, structures and covalently bound circular chromophoric dimers were studied to demonstrate the unusual spectral intensity reversal of the vibronic bands upon $\pi-\pi$ stacking. In Figure 1, both the primary molecular structures and secondary folded nanostructures are given, along with the degree of the spectral intensity reversal and its correlation to molecular self-organization.

The zeroth-order molecular exciton model[15] is commonly used to understand the solution and solid-state interactions of organic chromophores, assigning aggregate conformations on the basis of the energy of the Frenkel (molecular) absorption. Provided that the electronic transition is delocalized across the aggregate (i.e., strong electronic coupling between subunits), exciton effects will be observed wherein the subunit excited states split and strong spectral shifts of the absorption bands will occur relative to the monomeric chromophores. Assuming regular $\pi-\pi$ stacking, the conformations of organic aggregates are divided into two subgroups, H and J. H-aggregates are columnar, while J-aggregates exhibit either rotation or lateral slipping (offset) of each subunit. Relative to monomeric

(1) Gosztola, D.; Niemczyk, M. P.; Wasielewski, M. R. *J. Am. Chem. Soc.* **1998**, *120*, 5118.
(2) Zhao, Y.; Wasielewski, M. R. *Tetrahedron Lett.* **1999**, 40, 7047.
(3) Hayes, R. T.; Wasielewski, M. R.; Gosztola, D. *J. Am. Chem. Soc.* **2000**, *122*, 5563.
(4) Just, E. M.; Wasielewski, M. R. *Superlattices Microstruct.* **2000**, *28*, 317.
(5) Miller, S. E.; Zhao, Y.; Schaller, R.; Mulloni, V.; Just, E. M.; Johnson, R. C.; Wasielewski, M. R. *Chem. Phys.* **2002**, *275*, 167.
(6) Lukas, A. S.; Zhao, Y.; Miller, S. E.; Wasielewski, M. R. *J. Phys. Chem. B* **2002**, *106*, 1299.
(7) Giaimo, J. M.; Gusev, A. V.; Wasielewski, M. R. *J. Am. Chem. Soc.* **2002**, *124*, 8530.
(8) van der Boom, T.; Hayes, R. T.; Zhao, Y.; Bushard, P. J.; Weiss, E. A.; Wasielewski, M. R. *J. Am. Chem. Soc.* **2002**, *124*, 9582.
(9) Ahrena, M. J.; Fuller, M. J.; Wasielewski, M. R. *Chem. Mater.* **2003**, *15*, 2684.
(10) Andersson, M.; Sinks, L. E.; Hayes, R. T.; Zhao, Y.; Wasielewski, M. R. *Angew. Chem., Int. Ed.* **2003**, *42*, 3139.
(11) Wang, W.; Wan, W.; Stachiw, A.; Li, A. D. Q. *Biochemistry* **2005**, *44*, 10751.
(12) Wang, W.; Han, J. J.; Wang, L. Q.; Li, L. S.; Shaw, W. J.; Li, A. D. Q. *Nano Lett.* **2003**, *3*, 455.
(13) Wang, W.; Li, L. S.; Helms, G.; Zhou, H. H.; Li, A. D. Q. *J. Am. Chem. Soc.* **2003**, *125*, 1120.
(14) Wang, W.; Wan, W.; Zhou, H. H.; Niu, S. Q.; Li, A. D. Q. *J. Am. Chem. Soc.* **2003**, *125*, 5248.
(15) Kasha, M.; Rawls, H. R.; El-bayoumi, M. A. *Pure Appl. Chem* **1965**, *11*, 371.

10.1021/ja0687724 CCC: $37.00

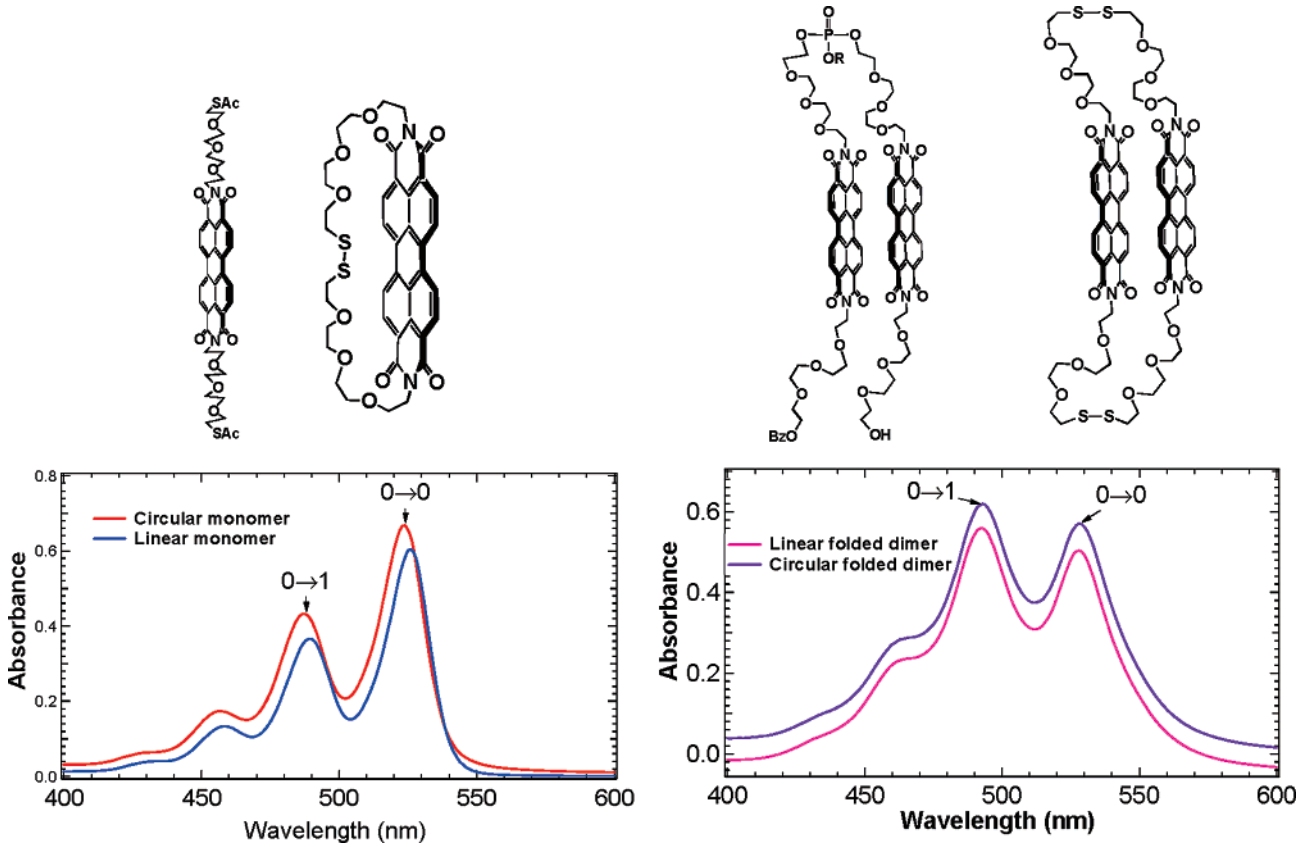

Figure 1. Absorption spectra of linear and circular perylene monomers (left). UV−vis spectra of folded and circular perylene linear dimers (right). Note the striking resemblance between monomer spectra and the dimer spectra, which reveal that optical properties mainly originate from folded π-stacks regardless of linear or circular construct.

absorption, exciton theory predicts that H-aggregation will lead to a blue shift in the lowest energy allowed electronic transition. J-aggregation is anticipated to only have a blue shift at small distortions from the H-aggregate structure and is typically associated with a red shift that correlates to the extent of displacement (see Supplementray Information).

This model describes exciton splitting solely by the relative dipole interactions of the subunit transitions without consideration of the aggregate electronic structure.[15] It also ignores coupling between vibrational and electronic transitions in spite of the well-known vibronic progression seen in Figure 1. Assuming that the electronic transition is coupled to a single vibration, the intensities of the vibrational transitions within the progression follow the order $0 \rightarrow 0 > 0 \rightarrow 1 > 0 \rightarrow 2$. The enhancement of the $0 \rightarrow 1$ and $0 \rightarrow 2$ bands upon aggregate formation leads to a red shift in the absorption maxima and is commonly attributed to Herzberg−Teller (HT) coupling in H-aggregates.[16] Thus, a correlation is commonly employed that relates vibronic band enhancement, position of the electronic transition, and aggregate geometry. Yet, as Figure 1 clearly shows, the position of the electronic transition is essentially unchanged upon dimer formation, and it would be anticipated that less-ordered J-aggregates would be more prevalent in solution than H-structures.

These experimental results demand a theoretical rendering beyond the exciton model, taking into account the explicit electronic structure and the coupling of vibrational and electronic transitions. The primary goal of this work is to examine the optical properties of gas-phase perylene tetracarboxylic diimide (PTCDI) chromophore aggregates as a function of conformation, comparing the excited-state distributions and transition intensities in the context of exciton and time-dependent density functional theory (TDDFT) in the strong electronic coupling regime. Our results indicate that the overall description given by exciton theory does not provide sufficient information to accurately characterize PTCDI aggregation on the basis of the position of the molecular electronic absorption. This has significant implications for the relatively routine experimental assignment of chromophore aggregation in PTCDI thin films on the basis of spectral shifts relative to the monomer absorption. Finally, we have calculated the relevant excited-state geometries and Franck−Condon factors to produce simulated spectra for the vibronic progression within the lowest energy optical transition of PTCDI monomer and dimer. On the basis of this data, we have assigned the vibrational modes that contribute to the progression. In addition to HT coupling, the displaced harmonic oscillator model is used to describe the marked vibronic enhancement in chromophoric dimers, and the source of the large excited-state geometric distortion is discussed.

Computational Methods

Athough the density functionals used in DFT cannot accurately describe the dispersion forces that contribute to the potential energy surface in π-bound systems,[17] recent studies have predicted reasonable

(16) Fulton, R. L.; Gouterman, M. *J. Chem. Phys.* **1961**, *35*, 1059.

(17) Sinnokrot, M. O.; Valeev, E. F.; Sherrill, C. D. *J. Am. Chem. Soc.* **2002**, *124*, 10887.

Scheme 1

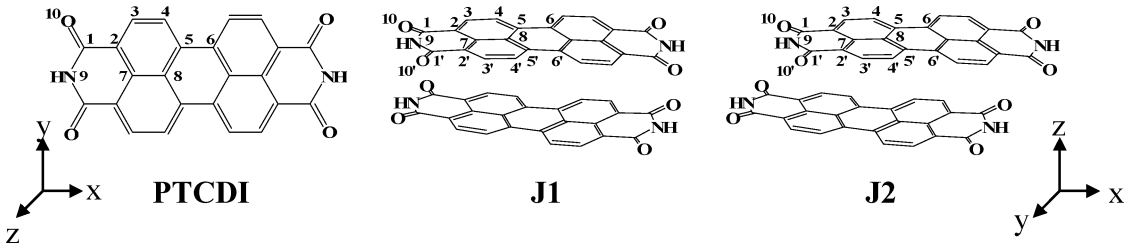

structures for $\pi-\pi$ dimers,[18] and it is likely that time-dependent DFT (TDDFT) will accurately predict the lowest energy excited states within perylene aggregates because of the correct molecular orbital (MO) description (vide infra). The geometries of the lowest energy singlet and triplet states of the 3,4,9,10-perylenetetracarboxylic diimide (PTCDI) monomer and cofacially stacked dimer were optimized with both the B3LYP[19] and BHandH[20] functionals and the 6-31G* basis set,[21−23] as implemented in Gaussian03.[24] The BHandH functional has recently been shown to yield π-stacked geometries similar to CCSD-(T) and MP2.[18] Normal-mode coordinate analysis confirmed each structure to be a local minima.[25]

The ground-state optical properties were first examined using TDDFT, which describes an excited state in terms of all possible single excitations from occupied to virtual orbitals. Natural transition orbital (NTO) analysis is used to convey the TDDFT results in a compact manner by way of rotation of the occupied and virtual orbitals, diagonalizing the transition density matrix that connects the ground and excited state.[26] The hole (H) and particle (P) orbitals represent the change in electron density during the excitation, and their eigenvalue represents the fraction of the total transition density that can be recovered by a particular hole−particle pair. Vibrational coupling to the lowest energy allowed electronic absorption was determined by the Franck−Condon (FC) factors, from the geometry difference between the ground and lowest energy triplet excited states, along with the ground normal modes for each using the BozeSuite program.[27−30] The method is exact within the harmonic approximation, incorporating potential surface displacements, mode frequency changes upon excitation, and mode mixing (Dushinsky effects).[31]

Results and Discussion

I. Geometry and Optical Properties of PTCDI Monomer. The ground-state optimized geometry of PTCDI is a planar D_{2h} structure that is nearly identical to that of 3,4,9,10-perylenetetracarboxylic dianhydride (PTCDA) except for those bond lengths and angles associated with the ring C−O bonds (Scheme 1, Table 1).[32,33] There are 108 internal molecular vibrational modes, 54 of them are Raman active ($19A_g + 18B_{3g} + 10B_{1g} + 7B_{2g}$), 46 are IR active ($18B_{1u} + 18B_{2u}\ 10B_{3u}$), and $8A_u$ modes are silent. Table 2 presents selected calculated vibrational modes, including symmetry assignments and IR intensities (complete tables in Supporting Information). Although modes $\nu_{81}-\nu_{89}$ have energies comparable to the band separation within the observed vibrational progression,[12−14] none are totally symmetric which prevents their coupling to the dipole-allowed optical transition. Previously, the vibronic progression has been interpreted in terms of a configuration coordinate diagram for a single effective vibrational mode of the molecule, however,

Table 1. Selected Bond Lengths (Å) and Angles (°) for the Optimized Ground and Lowest Energy Triplet State Geometries of PTCDI Monomer and the **J1** and **J2** Conformations of the PTCDI Dimer[a]

	PTCDI	**J1**	**J2**
state	$1\,^1A_g$	$1\,^1A_1$	$1\,^1A$
B3LYP E	−1331.1244	−2662.2497	−2662.2505
B3LYP E_{ZPE}^{298}	−1330.5306	−2661.0606	−2661.0607
BHandH E	−1321.8637	−2643.7110	−2643.7125
BHandH E_{ZPE}^{298}	−1321.2183	−2642.4720	−2642.4735
interplane dist.		3.6−4.1 (3.0−3.4)	3.4−4.0 (3.0−3.5)
rotation		29 (30)	31 (33)
offset in x		0 (0)	2 (2)
$r_{1,2}$	1.483 (1.464)	1.484 (1.465)	1.482 (1.466)
$r_{2,3}$	1.383 (1.363)	1.383 (1.363)	1.383 (1.364)
$r_{3,4}$	1.399 (1.387)	1.399 (1.388)	1.399 (1.388)
$\alpha_{1,2,7}$	120.77 (120.63)	120.71 (120.55)	120.63 (120.23)
$\alpha_{2,1,10}$	124.04 (123.45)	123.78 (123.00)	123.88 (122.65)
$\alpha_{4,5,6}$	122.14 (121.97)	122.18 (122.01)	122.17 (121.96)
$\omega_{5,8,5,6}$		3.71 (1.44)	4.22 (3.26)
$\omega_{4,5,8,7}$		3.09 (1.38)	3.51 (1.21)
	$1\,^3B_{3u}$	$1\,^3B_1$	$1\,^3A$
B3LYP E	−1331.0760	−2662.1932	−2662.1935
B3LYP E_{ZPE}^{298}	−1330.4873	−2661.0061	−2661.0064
BHandH E	−1321.7874	−2643.6466	−2643.6466
BHandH E_{ZPE}^{298}	−1321.1759	−2642.4076	−2642.4077
interplane dist.		3.6−3.8 (3.0−3.3)	3.4−4.5 (3.0−3.4)
rotation		40 (37.2)	28 (38)
offset in x		0 (0)	1 (0)
$r_{1,2}$	1.475 (1.457)	1.479 (1.460)	1.479 (1.460)
$r_{2,3}$	1.408 (1.393)	1.396 (1.378)	1.396 (1.378)
$r_{3,4}$	1.373 (1.357)	1.385 (1.372)	1.386 (1.372)
$\alpha_{1,2,7}$	120.80 (120.64)	120.80 (120.62)	120.82 (120.62)
$\alpha_{2,1,10}$	123.85 (123.22)	123.77 (123.13)	123.70 (123.13)
$\alpha_{4,5,6}$	122.24 (122.14)	122.25 (122.28)	122.23 (122.28)
$\alpha_{5,8,5,6}$	0.00 (0.00)	2.47 (0.86)	4.30 (0.90)
$\omega_{4,5,8,7}$	0.00 (0.00)	1.60 (4.90)	3.62 (4.90)

[a] B3LYP values are presented, BHandH in parentheses. The total DFT electronic energy (E) in addition to the zero point and thermally corrected value (E_{298}^{ZPE}) is given in hartrees (1 hart. = 627.509541 Kcal/mol).

(18) Waller, M. P.; Robertazzi, A.; Platts, J. A.; Hibbs, D. E.; Williams, P. A. *J. Comput. Chem.* **2006**, *27*, 491.
(19) Becke, A. D. *Phys. Rev. A* **1988**, *38*, 3098. Lee, C.; Yang, E.; Parr, R. G. *Phys. Rev. B* **1988**, *37*, 785.
(20) Becke, A. D. *J. Chem. Phys.* **1993**, *98*, 1372.
(21) Francl, M. M.; Petro, W. J.; Hehre, W. J.; Binkley, J. S.; Gordon, M. S.; DeFree, D. J.; Pople, J. A. *J. Chem. Phys.* **1982**, *77*, 3654.
(22) Harihan, P. C.; Pople, J. A. *Theor. Chim. Acta* **1973**, *28*, 213.
(23) Rassalov, V.; Pople, J. A.; Ratner, M.; Windus, T. L. *J. Chem. Phys.* **1998**, *109*, 1223.
(24) Frisch, M. J.; et al. *Gaussian03*, Rev C.01; Gaussian, Inc.: Pittsburgh, PA, 2003.
(25) No imaginary vibrations or a single frequency below −15 cm^{-1} was observed. Unless high-precision frequencies are requested, small negative vibrations may be present in large systems such as these. (See Supplementary Information.)
(26) Batista, E. R.; Martin, R. L. *Encyclopedia of Computational Chemistry*; John Wiley and Sons Ltd.: Chichester, U.K., 2003. Martin, R. L. *J. Chem. Phys.* **2003**, *118*, 4775.
(27) Short, K. W.; Callis, P. R. *J. Chem. Phys.* **2000**, *113*, 5235.
(28) Short, K. W.; Callis, P. R. *Chem. Phys.* **2002**, *283*, 269.
(29) Doktorov, E. V.; Malkin, I. A.; Man'ko, V. I. *J. Mol. Spectrosc.* **1975**, *56*, 1.
(30) Doktorov, E. V.; Malkin, I. A.; Man'ko, V. I. *J. Mol. Spectrosc.* **1977**, *64*, 302.
(31) Dushinsky, F. *URSS* **1937**, *7*, 551.
(32) Kobitski, A. Y.; Scholz, R.; Zahn, D. R. T. *J. Mol. Struct.: THEOCHEM* **2003**, *625*.
(33) Zhanpeisov, N. U.; Nishio, S.; Fukumura, H. *Int. J. Quantum Chem.* **2005**, *105*, 368.

Table 2. B3LYP Vibrational Frequencies and Assignments for Selected Modes, ν, of PTCDI Monomer[a]

vib	sym.	*E*	*I*		vib.	sym.	*E*	*I*	
ν_{12}	A_g	231	0	in-plane ν_{C-C}	ν_{76}	B_{2u}	1297	232	in-plane ν_{C-C}, δ_{C-H}
ν_{18}	B_{1u}	369	68	in-plane $\nu_{C=O}$	ν_{77}	A_g	1308	0	in-plane ν_{C-C}, δ_{C-H}
ν_{24}	B_{1u}	463	54	in-plane δ_{C-C-C}	ν_{81}	B_{1u}	1366	488	in-plane ν_{C-C}, δ_{C-H}
ν_{30}	A_g	550	0	in-plane δ_{C-C-C}	ν_{83}	B_{1u}	1390	299	in-plane ν_{C-C}, δ_{C-H}
ν_{37}	B_{1u}	667	49	in-plane δ_{C-C-C}	ν_{86}	B_{2u}	1422	31	in-plane δ_{N-H}
ν_{40}	B_{3u}	709	43	in-plane δ_{N-H}	ν_{88}	B_{1u}	1436	55	in-plane ν_{C-C}
ν_{47}	B_{3u}	756	203	out-of-plane δ_{N-H}	ν_{89}	B_{1u}	1464	155	in-plane ν_{C-C}, δ_{C-H}
ν_{51}	B_{1u}	811	34	in-plane δ_{C-C-C}	ν_{99}	B_{1u}	1646	646	in-plane ν_{C-C}, δ_{C-H}
ν_{57}	B_{3u}	867	72	out-of-plane δ_{C-H}	ν_{100}	B_{3g}	1660	0	in-plane ν_{C-C}
ν_{59}	B_{1u}	966	32	in-plane δ_{C-C-H}	ν_{102}	B_{2u}	1786	944	in-plane $\nu_{C=O}$, δ_{N-H}
ν_{66}	B_{2u}	1129	40	in-plane δ_{C-C-H}, δ_{N-H}	ν_{103}	B_{1u}	1786	981	in-plane $\nu_{C=O}$
ν_{72}	B_{2u}	1215	85	in-plane δ_{C-C-H}, δ_{N-H}	ν_{113}	B_{1u}	3582	182	in-plane ν_{N-H}

[a] Energy (*E*) in cm^{-1}, IR intensities (*I*) in KM/mol. Band stretches are indicated by ν_{A-B}, while wags and torsions are shown by δ_{A-B}.

Table 3. Lowest Four Singlet Excited States of PTCDI, **J1** and **J2**, Calculated by TD-B3LYP and TD-BHandH (in Parentheses)[a]

state	configuration	C	*E* (nm)	*f*
		PTCDI (D_{2h})		
$^1B_{3u}$	H → L	0.6 (0.6)	504.93 (432.35)	0.6 (0.8)
$^1B_{1u}$	H-1 → L	0.7 (0.6)	416.49 (310.08)	0.0 (0.0)
$^1B_{2g}$	H-2 → L	0.7 (0.6)	395.76 (290.46)	0.0 (0.0)
$^1B_{1g}$	H-3 → L (H-4 → L)	0.6 (0.5)	395.41 (291.54)	0.0 (0.0)
		J1 (D_2)		
$^1B_1$	H → L	0.6 (0.6)	607.05 (493.55)	0.0 (0.0)
	H-1 → L + 1	−0.4 (0.1)		
$^1B_3$	H-1 → L	0.5 (−0.5)	602.04 (437.90)	0.0 (0.0)
	H → L + 1	−0.5 (0.5)		
$^1B_1$	H-1 → L + 1	0.6 (0.7)	530.53 (414.57)	0.1 (0.0)
$^1B_3$	H → L + 1	0.4 (0.5)	488.13 (416.02)	0.9 (1.0)
	H-1 → L	0.4 (0.4)		
		J2 (C_2)		
^1A	H-1 → L + 1	−0.5 (−0.2)	604.23 (487.92)	0.0 (0.0)
	H → L	0.5 (0.6)		
^1A	H-1 → L	−0.5 (0.4)	603.58 (445.43)	0.0 (0.0)
	H → L + 1	0.5 (0.6)		
^1A	H-1 → L + 1	0.5 (0.6)	535.23 (434.48)	0.1 (0.0)
^1A	H-1 → L	0.4 (0.6)	490.73 (423.58)	0.9 (1.0)
	H → L + 1	0.4 (−0.3)		

[a] The dominant configurations (HOMO = H, LUMO = L), their coefficients (*C*), energy (nm), and oscillator strength (*f*) are presented.

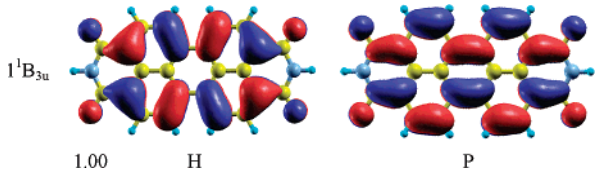

Figure 2. Natural transition hole (H) and particle (P) orbitals for the 1 $^1B_{3u}$ state of PTCDI monomer as determined from TD-B3LYP/6-31G*. The NTO coefficients represent the extent to which the excitation can be written as a single configuration.

the lack of symmetry in modes $\nu_{81}-\nu_{89}$ indicates that transitions within multiple vibrations must contribute to the observed structure.

The lowest energy allowed electronic transition is predicted by TD-B3LYP to be the 1 $^1B_{3u}$ state at 505 nm (Table 3). In general, all TD-BHandH excitation energies are higher in energy relative to that predicted by B3LYP by ∼60−100 nm. The B3LYP excitation energy agrees well with the UV−vis absorption of a variety of PTCDI derivatives, which exhibit electronic excitation between 500 and 550 nm.[34,35] Absorption is dominated by a HOMO → LUMO transition, and the NTOs, which capture the change in electron density upon excitation, are nearly identical to these orbitals (Figure 2). The lowest energy triplet state from which phosphorescence would be expected is the 1 $^3B_{3u}$ at 992 nm. Examination of the NTOs for both the triplet and singlet B_{3u} states indicates that they have the same electronic structure differing only in the total spin. We therefore optimized the geometry of the B3LYP 1 $^3B_{3u}$ state and used that as an approximation for the excited-state geometry of the 1 $^1B_{3u}$. The triplet geometry exhibits pronounced bond length alternation relative to the ground state, with contraction of those C−C bonds that lie along the long axis (*x*) and lengthening of alternate C−C bonds (Table 1). This structure is comparable to the optimized excited-state geometry of PTCDA determined by the density-functional tight-binding method and resonance Raman vibrational enhancement.[34]

The vibronic structure in the UV−vis spectra of PTCDI results from the simultaneous excitation of the electronic transition and one (or more) vibrational modes. Experimentally, the spacing of the vibronic progression is ∼1400 cm^{-1} for a variety of PTCDI derivatives (the experimental error is ±40 cm^{-1} in this energy region). Coupling of vibrational and electronic excitations is determined by the Franck−Condon (FC) factors, whose calculation requires an accurate description of the geometries and potential energy surfaces (PES) of the two electronic states involved. Using the B3LYP optimized geometries of the ground and 1 $^3B_{3u}$ states, the FC factors for each vibrational mode were calculated and the progression associated with the first electronic absorption at 505 nm was simulated. To assess the dependence of the vibrational structure upon symmetry, the FC factors were determined under both the D_{2h} and C_1 representations. In the former, only totally symmetric vibrations (A_g) should be elongated under the dipole-allowed HOMO → LUMO transition, leading to large FC factors. However, lifting the symmetry should facilitate the participation of lower order vibrations to the spectrum (e.g., *xy* polarized B_{3g} modes).

The B3LYP C_1 spectrum for excitation to the 1 $^1B_{3u}$ state, shown in Figure 3, exhibits good agreement with the experimental absorption spectrum of ethylene glycol substituted PTCDI.[13] Quite similar results are obtained with the BHandH functional. Four bands are observed in both cases and the interpeak spacing ranges from 1238 to 1398 cm^{-1}, which is well within the energy range for perylene C−C stretches. As each peak has a full width at half-maximum (fwhm) of 200

(34) Scholz, R.; Kobitski, A. Y.; Kampen, T. U.; Schreiber, M.; Zahn, D. R. T.; Jungnickel, G.; Elstner, M.; Sternberg, M.; Frauenheim, T. *Phys. Rev. B* **2000**, *61*, 13659.
(35) Ahrens, M. J.; Fuller, M. J.; Wasielewski, M. R. *Chem. Mater.* **2003**, *15*, 2684.

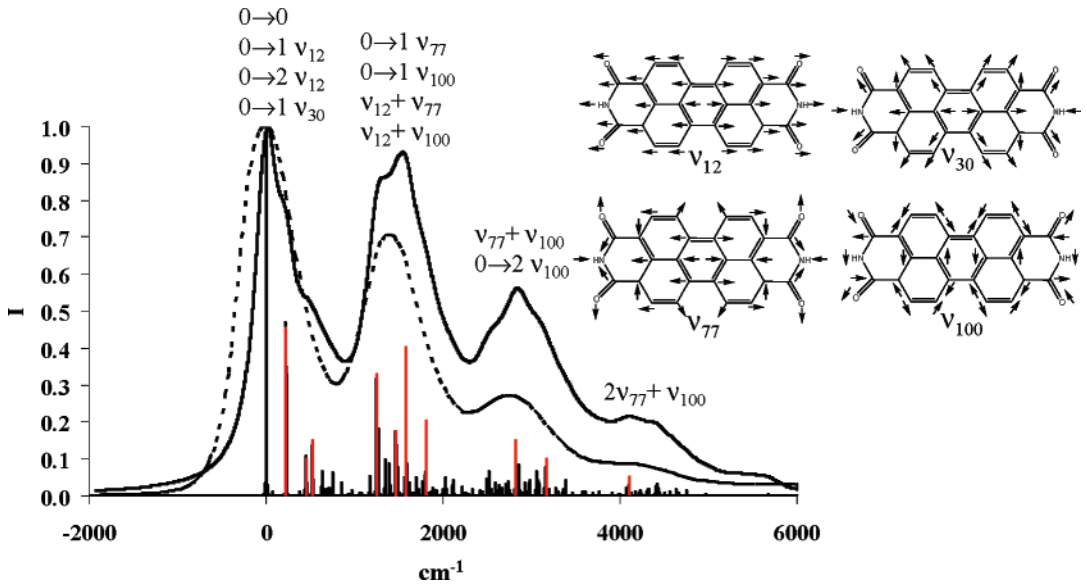

Figure 3. Simulated B3LYP electronic absorption spectra (solid, sticks) for gas-phase PTCDI (excitation to the 1 $^1B_{3u}$ state) and experimental spectra (dot) of ethylene glycol substituted PTCDI.[13] Contributing modes are inset and highlighted in red.

cm^{-1}, several vibrational transitions occur within each band, generating an overall spacing of nearly 1400 cm^{-1}. The first peak at 505 nm (set to zero cm^{-1} in Figure 3) contains not only the 0 → 0 transition but also the 0 → 1 and 0 → 2 transitions for ν_{12} as well as the 0 → 1 transition for ν_{30} (Table 2). The second peak at 1398 cm^{-1} has contributions from the 0 → 1 transitions of mode ν_{77} as well as mode ν_{100} in addition to two combination bands $\nu_{12} + \nu_{77}$ and $\nu_{12} + \nu_{100}$.

The third peak in the progression, at 2742 cm^{-1}, is dominated by a combination band $\nu_{77} + \nu_{100}$ as well as the 0 → 2 transition for ν_{100}. Finally, the largest contributor to the fourth band at 4300 cm^{-1} is from the combination $2\nu_{77} + \nu_{100}$. A qualitatively similar spectrum is observed when the FC calculation is performed under D_{2h} symmetry, yet the B_{3g} mode, ν_{100}, does not contribute to the observed structure. These results are in good agreement with previous FC calculations that examined the geometrical distortions upon the optical excitation of PTCDA.[34]

II. Optical Properties of Idealized PTCDI Aggregate. The TDDFT excited-state description takes into account the effect of electronic structure on exciton splitting and, at an idealized aggregate geometry, can be considered a first-order correction to the zeroth-order exciton model. To investigate differences between the first- and zeroth-order descriptions, in the absence of vibrational coupling and geometric relaxation,[15] we examined the TDDFT excited-state distributions within classic H- and J-dimer aggregates as a function of conformation (interplanar separation, rotation, and offset along both the short and long axes), with each subunit at the optimized monomer geometry. In general, caution must be exercised when using TDDFT to describe the excited states of chromophore aggregates, as charge transfer (CT) character within an electronic excitation is not well described by the TDDFT method.[36] Although CT transitions are considered to play a large role in the optical behavior of crystalline PTCDI thin films, a recent resonance Raman and theoretical study has indicated that the lowest energy transition within PTCDI derivatives (3.2−3.5 Å interplanar separation) is molecular in nature, with little to no CT character.[34] In this paper, we are primarily concerned with the lowest energy optical absorption of PTCDI dimer, and TDDFT should accurately describe this excitation.

Under D_{2h} symmetry, the frontier orbital electronic configuration that should contribute to the optical spectra of the cofacially stacked dimer is $...b_{1g}^2a_u^2b_{2u}^0b_{3g}^0$, where each MO is a linear combination of the monomer orbitals. The a_u HOMO is derived from the HOMO + HOMO combination of the PTCDI monomer orbitals (hereafter referred to $PTCDI_{HOMO}$ + $PTCDI_{HOMO}$) which are each of a_u symmetry, while the HOMO-1 b_{1g} orbital is formed from the corresponding negative linear combination (for an example, see the hole and particle NTOs of Figure 2 and Figure 7). The b_{2u} LUMO orbital derives from the $PTCDI_{LUMO}$−$PTCDI_{LUMO}$ combination of the monomer orbitals, each of which are of b_{1g} symmetry, and the LUMO+1 orbital comes from the analogous $PTCDI_{LUMO}$ + $PTCDI_{LUMO}$. In the following, TD-B3LYP results are presented, however, the same trends are observed using the BHandH functional.

H-Dimers. Starting with the eclipsed H-dimer of D_{2h} symmetry, TDDFT calculations and NTO analyses were performed at subunit separations (d) between 3.0 and 30.0 Å (Figure 4). At each distance, the lowest four singlet excited states (1−2 $^1B_{1g}$, 1−2 $^1B_{3u}$) were determined to be linear combinations of the allowed HOMO → LUMO transition of PTCDI monomer. The optically allowed state is the 2 $^1B_{3u}$, which at small distances is multiconfigurational, with two hole−particle pairs representing $PTCDI_{HOMO}$ + $PTCDI_{HOMO}$ → $PTCDI_{LUMO}$ + $PTCDI_{LUMO}$ and $PTCDI_{HOMO}$−$PTCDI_{HOMO}$ → $PTCDI_{LUMO}$−$PTCDI_{LUMO}$ transitions. Thus, in the experimentally relevant strong electronic coupling regime, the excitation is completely delocalized across both subunits. At long interplanar separation, the wave function remains multiconfigurational but with each configuration reducing to the HOMO → LUMO transition on individual subunits. This is relevant, as intermediate to weak electronic coupling between chromophoric centers localizes the excitation.

(36) Dreuw, A.; Head-Gordon, M. *J. Am. Chem. Soc.* **2004**, *126*, 4007.

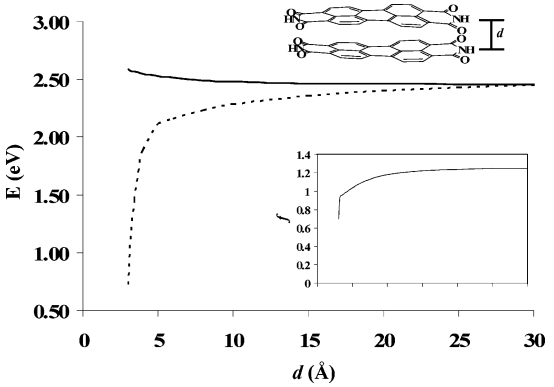

Figure 4. Energy (eV) of the forbidden 1 ^1B_g (dot) and allowed 2 $^1B_{3u}$ (solid) states in D_{2h} H-aggregate PTCDI dimer, as a function of interplanar separation, *d* (each subunit at the monomer geometry). Oscillator strength, *f*, for the allowed state inset. Sixteen total data points were used, taken every 0.2 Å from 3 to 4 Å separation, every 1.0 Å from 5 to 10 Å separation, and every 5 Å thereafter.

The forbidden exciton state is the lower energy 1 $^1B_{1g}$, which may be attributed to a $PTCDI_{HOMO} + PTCDI_{HOMO} \rightarrow PTCDI_{LUMO}-PTCDI_{LUMO}$ transition at short intermolecular separation. Electronic absorption in the H-dimer to the allowed 2 $^1B_{3u}$ state leads to a blue shift (22 nm at $d = 3.5$ Å) relative to the lowest energy excitation of the monomer. This is in agreement with Kasha's exciton model, which predicts that the higher energy exciton state is allowed because the in-phase dipole interaction of the two subunits yields a nonzero transition moment, while the out-of-phase dipole arrangement (the lower energy exciton state) leads to zero transition moment (see Supporting Information). The exciton state splitting for the 2 $^1B_{3u}$ and 1 $^1B_{1g}$ states is shown in Figure 4.

Laterally Displaced J-Aggregates. Kasha's original work investigated the exciton splitting of "in-line" dimers with those of cofacially stacked systems. There, the allowed and forbidden states should exhibit an oscillatory dependence, with the two states crossing along the displacement coordinate. Small displacements are expected to lead to a blue shift, while larger displacements red shift the absorption relative to the monomer (Supporting Information).[15]

Here, we examine lateral motion along both the short (*y*) and long (*x*) axes of the PTCDI subunit (Scheme 1). Formally, either displacement decreases the symmetry of the system to C_{2h}, leading to two pairs of allowed and forbidden exciton states in the TDDFT description. In the case of lateral motion along the long axis, these states are the first and second ^1A_g and ^1B_u, which derive from the HOMO → LUMMO transition of PTCDI and are analogous to those discussed for H-dimer. The energies of the allowed ^1B_u and forbidden ^1A_g states as a function of offset are presented in Figure 5A. Within the 0−5 Å offset regime, transition to the 2 ^1B_u state will dominate the electronic spectrum, as its oscillator strength is nearly 3 times that of secondary allowed 1 ^1B_u state. From 0 to 3 Å, the 2 $^1B_u \leftarrow$ 1 ^1A_g transition will be blue-shifted (from 22 to 41 nm) relative to electronic absorption of PTCDI monomer. Beyond this point, the electronic absorption is nearly the same energy as the monomer, until an offset value of 5.5 Å is reached and the absorption red shifts slightly (<10 nm).

Lateral displacement along the short axis (*y*) changes the highest symmetry axis such that the allowed exciton states are the first and second ^1A_u, while the forbidden states are the

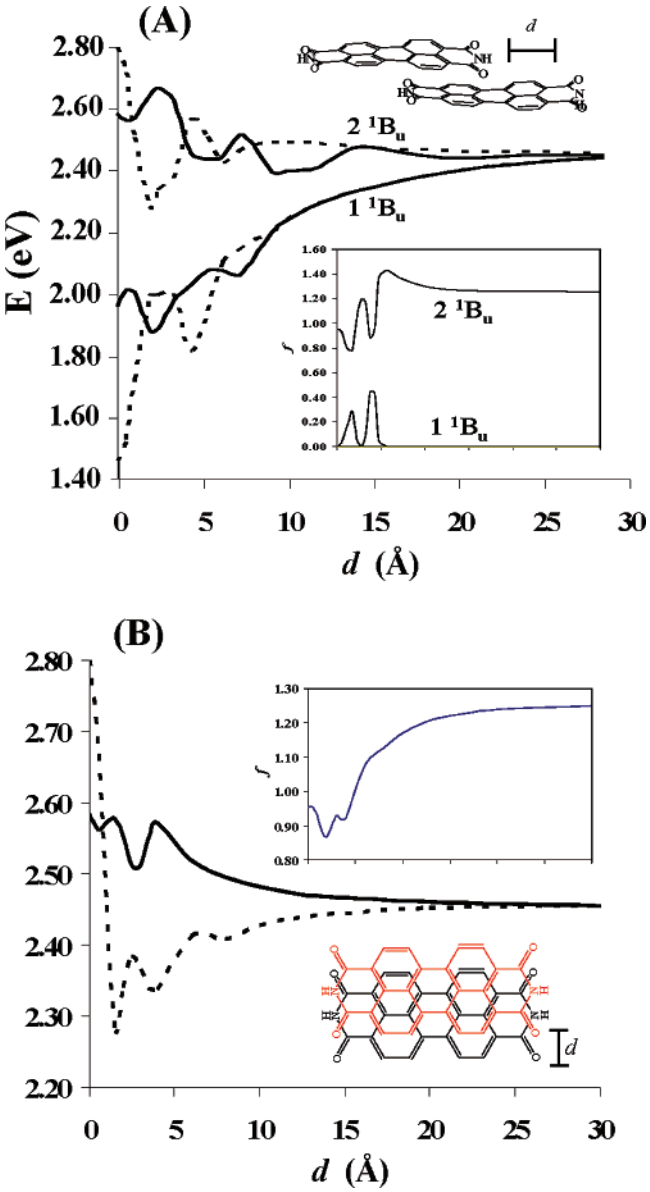

Figure 5. (A) Energy (eV) of the forbidden ^1A_g (dot) and allowed ^1B_u states (solid) in C_{2h} J-aggregate PTCDI dimer, as a function of lateral motion, *d*, along the long molecular axis; (B) energy (eV) of the forbidden 2 ^1B_g (dot) and allowed 2 ^1A_u (solid) states, as a function of lateral displacement along the short PTCDI axis (each subunit at the monomer geometry). Oscillator strength, *f*, inset. Interplanar distance between subunits is 3.5 Å. Twenty-four data points total, taken every 0.5 Å from 0 to 10 Å displacement and every 5 Å thereafter.

first and second ^1B_g. In this case, the oscillator strength of the 1 ^1A_u is close to zero along the displacement coordinate, and so only the 2 ^1A_u and 2 ^1B_g pair of exciton states will be discussed. Figure 5B illustrates the energies of the allowed 2 ^1A_u and the forbidden 2 ^1B_g states as a function of displacement. Unlike offset in the *x*-direction, motion along *y* leads to a blue shift across the entire displacement coordinate. Within the regime of experimental interest (offset up to 3 Å), the absorption is between 22 and 10 nm higher in energy than in the monomer.

Rotationally Displaced J-Aggregates. Rotation of one PTCDI subunit can be performed under D_2 symmetry, which leads to a single pair of exciton allowed (2 $^1B_3$) and forbidden (1 $^1B_1$) states. These are the reduced symmetry analogues of

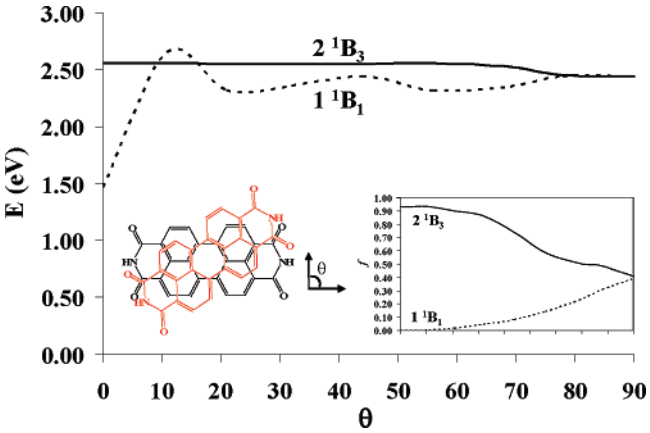

Figure 6. Energy (eV) of the forbidden 1 $^1B_1$ (dot) and allowed 2 $^1B_3$ (solid) states in D_2 J-aggregate PTCDI dimer (each subunit at the monomer geometry) as a function of rotation, θ. Oscillator strength, f, as a function of rotation, θ, inset. Interplanar distance between subunits is 3.5 Å. Nineteen data points total taken every 5°.

the 2 $^1B_{3u}$ and 1 $^1B_{1g}$ states in the classic H-dimer. Importantly, rotation alters the allowedness of the 2 $^1B_3$ and 1 $^1B_1$ states because the dipole interaction of the subunit transitions changes as a function of theta. This is clearly manifested in both the excited-state energies and the relative oscillator strengths of the two states, as shown in Figure 6. As one subunit is rotated relative to the other, the energy of the "forbidden" 1 $^1B_1$ state increases until it has the same energy as the "allowed" 2 $^1B_3$ state at $\theta = 90°$. Similarly, the oscillator strength of the forbidden state increases until both the $^1B_1$ and 2 $^1B_3$ have the same f-values at $\theta = 90°$, where the dipole interactions of the $PTCDI_{HOMO} + PTCDI_{HOMO} \rightarrow PTCDI_{LUMO} + PTCDI_{LUMO}$ and $PTCDI_{HOMO} + PTCDI_{HOMO} \rightarrow PTCDI_{LUMO} - PTCDI_{LUMO}$ transitions for each state become equivalent.

The TDDFT results presented above are most closely correlated to the thin film systems, where it is well-known that PTCDI chromophores remain essentially planar and exhibit regular stacking geometries. These predictions indicate that the energy of the Frenkel transition may not be a good indicator of oligomer conformation in the solid state, as multiple conformations yield the same observable. Although zeroth-order molecular exciton theory typically holds that moderate distortions away from the high-symmetry H-aggregate will red shift the lowest energy transition relative to the monomer absorption, TDDFT instead predicts that no shifting or blue-shifting is typical of nearly all J-aggregate geometries. In the following section, the optical properties of optimized PTCDI dimers are discussed, the results of which should more closely correlate to the UV−vis of perylene aggregates in solution.

III. Optical Properties of Optimized PTCDI Dimers. Geometry. To fully explore the conformational PES of PTCDI dimer, three single-point PES scans were performed that examined (1) rotation, θ, of one subunit, (2) offset, d, of one subunit along the long axis, and (3) offset, d', of one subunit along the short axis. Full geometry optimizations of two conformations (**J1**−**J2**) were then performed at starting geometries with $d = 0$ Å and $\theta = 30°$ (**J1**) and at $d = 2$ Å with $\theta = 30°$ (**J2**) (Scheme 1). As seen in Table 1, the **J1** conformation maintained zero offset and optimized to $\theta = 29°$, with a B3LYP intermolecular separation between 3.6 and 4.1 Å owing to dihedral angle rotation of each subunit toward its partner by 8°. The **J2** structure optimized to a 2 Å offset (along the long axis) with 31° rotation and similar bowing of the subunits toward each other. Bond length and angle differences between **J1** and **J2** are minimal, with the primary structural deviations being the lateral position in x. Both **J1** and **J2** have intermolecular separations that are similar to solid-state experimental values for a variety of perylene thin films, however, the BHandH functional consistently predicts ~0.5 Å smaller interplanar separation than B3LYP. Relative to the monomer geometry, the dominant distortion of each subunit involves the dihedral motion of the phenyl rings toward the complementary subunit. B3LYP predicts that the **J2** conformation is 0.55 kcal/mol lower in energy than the **J1** isomer and that the interaction energies ($E_{dimer} - 2E_{monomer}$) are 1.0 and 0.6 kcal/mol, respectively. The BHandH functional predicts the gas-phase dimer to be much more strongly bound, with interaction energies of 24.0 and 25.0 kcal/mol for **J1** and **J2**, respectively. The basis set superposition errors for the B3LYP results are ~4 kcal/mol, which means that taking into account this correction makes **J1** and **J2** unbound species. In contrast, the BSSE correction for the BHandH results is nearly 9 kcal/mol, which leads to interaction energies of 13.3 and 13.09 kcal/mol for **J1** and **J2**. Previous experimental results have determined the interaction energy between PTCDI dimers to be 2−7 kcal/mol in $C_2H_2Cl_4$.[18−20] Thus, it appears that the B3LYP functional underestimates the interaction between subunits, while the BHandH function overestimates this value. Nevertheless, as will be shown throughout this work, there is no qualitative difference between the conclusions drawn from either functional.

There are 234 internal molecular vibrational modes present in the PTCDI dimer. Assuming D_2 symmetry, as in **J1**, 234 of them are Raman active (60A + 58B + $58B_2$ + $58B_3$), 174 of them are IR active ($58B_1$ + $58B_2$ + $58B_3$), and 60 of them are IR (60A) silent. Assuming C_2 symmetry, as in **J2**, all modes are Raman and IR allowed (118A + 116B), however, only 38 (11A + 27B) and 53 (28A + 25B) modes exhibit significant Raman and IR intensity, respectively. Table 4 presents selected calculated vibrational modes, including symmetry assignments and IR intensities. A complete table of frequencies is given in the Supporting Information. Owing to the structural similarities between **J1** and **J2** and PTCDI monomer, the predicted IR and Raman spectra between the three systems are nearly identical. Indeed, the only significant difference between the predicted vibrational frequencies and intensities lies in the out-of-plane C−C bends, which occur at ~780 cm^{-1} in the two dimers and at ~810 cm^{-1} in the monomer.

Optical Properties in the Strong Electronic Coupling Limit. Having considered the exciton splitting of idealized PTCDI dimers, allowing for electronic effects and symmetry breaking in the intermediate to weak electronic coupling regime, we now turn to the spectral properties of the optimized **J1** and **J2** conformations. In the **J1** structure (D_2 symmetry), the allowed electronic transition is predicted by TD-B3LYP to be at 488 nm (2.54 eV), populating the 2 $^1B_3$ exciton state, while the **J2** conformation is predicted to have an absorption at 491 nm (2.53 eV) to the 4 ^1A exciton state (Table 3). Thus, blue shifts of 17 and 14 nm are predicted for the B3LYP **J1** and **J2** electronic excitations relative to that of the monomer. Using the BHandH functional, blue shifts of 16 and 9 nm are observed for **J1** and **J2**, respectively. These shifts are slightly less than

Table 4. Selected B3LYP Vibrational Frequencies and Assignments for **J1** and **J2** PTCDI Dimers[a]

vib	sym.	freq.	I		vib.	sym.	freq	I	
				J1 (D_2)					
ν_{85}	B_2	700	122	out-of-plane δ_{N-H}	ν_{204}	B_1	1646	806	in-plane ν_{CC}
ν_{96}	B_2	751	418	out-of-plane δ_{N-H}	ν_{207}	B_1	1782	528	in-plane $\nu_{C=O}$
ν_{118}	B_2	865	151	out-of-plane δ_{C-H}	ν_{209}	B_3	1785	109	in-plane $\nu_{C=O}$
ν_{158}	B_1	1298	330	in-plane ν_{C-C}, ν_{C-N}	ν_{211}	B_1	1787	1091	in-plane $\nu_{C=O}$
ν_{168}	B_3	1368	629	in-plane ν_{C-C}	ν_{212}	B_3	1787	1366	in-plane $\nu_{C=O}$
ν_{172}	B_3	1391	402	in-plane ν_{C-C}, δ_{C-H}	ν_{233}	B_3	3582	373	In-plane ν_{N-H}
ν_{184}	B_3	1464	203	in-plane ν_{C-C}					
				J2 (C_2)					
ν_{96}	B	754	224	out-of-plane δ_{N-H}	ν_{207}	A	1777	247	in-plane $\nu_{C=O}$
ν_{97}	B	756	198	out-of-plane δ_{N-H}, δ_{C-C}	ν_{208}	B	1779	360	in-plane $\nu_{C=O}$
ν_{118}	B	865	125	out-of-plane δ_{C-H}	ν_{210}	B	1786	691	in-plane $\nu_{C=O}$
ν_{158}	A	1298	332	in-plane ν_{C-C}, ν_{C-N}	ν_{211}	B	1786	216	in-plane $\nu_{C=O}$
ν_{168}	B	1367	621	in-plane ν_{C-C}	ν_{212}	A	1787	1339	in-plane $\nu_{C=O}$
ν_{172}	B	1389	439	in-plane ν_{C-C}, δ_{C-H}	ν_{213}	B	1790	267	in-plane $\nu_{C=O}$
ν_{184}	B	1463	215	in-plane ν_{C-C}	ν_{231}	B	3576	155	in-plane ν_{N-H}
ν_{204}	B	1646	831	in-plane ν_{C-C}	ν_{233}	B	3585	192	in-plane ν_{N-H}

[a] Energy (E) in cm^{-1}, IR Intensities (I) in KM/mol.

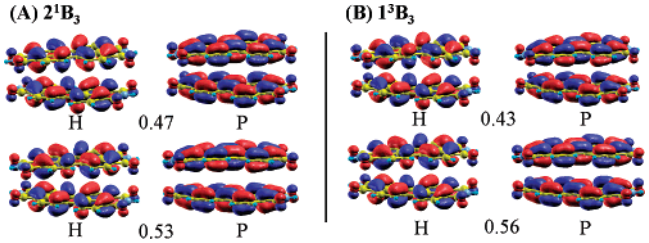

Figure 7. TD-B3LYP/6-31G* hole (H) and particle (P) natural transition orbitals for (A) the allowed singlet exciton state and (B) the lowest energy triplet states of **J1**. The NTO coefficients represent the extent to which the excitation can be written as a single configuration.

that predicted in the ideal PTCDI structures, indicating that geometric relaxation somewhat decreases the magnitude of exciton splitting. As seen in Table 3, the 2 $^1B_3$ state of **J1** and the 4 ^1A state of **J2** are both dominated by equal contributions from the HOMO-1 → LUMO and HOMO → LUMO+1 configurations within the TDDFT description. Natural transition orbital analysis of **J1** reveals that these two states are biconfigurational, yielding two hole−particle pairs for each state, as shown in Figure 7. Similar results are obtained for **J2**.

In chromophoric aggregates, there is a balance between two mechanisms which participate in vibrational coupling to an electronic transition, leading to vibronic band enhancement. The first, Herzberg−Teller (HT) coupling,[16] is typically considered in H-aggregates of D_{2h} symmetry. As a result of the high symmetry of the system, only the totally symmetric vibrational modes, which were active in the monomer excitation, are displaced upon dipole-allowed optical excitation. In the dimer, there are + and − combinations of the totally symmetric modes of each subunit, the latter of which removes the electronic degeneracy of the H-dimer and to first order mixes the allowed and forbidden exciton states linearly in the displacement. As such, the forbidden exciton state can exhibit an intense absorption, however, the origin of its vibrational progression is displaced in energy by one quantum of the mode responsible for mixing the exciton states. HT coupling is operative in J-aggregates, however, it does not lead to intensity reversal of the vibronic bands. The displaced harmonic oscillator model is a second construct for interpreting the changes in the intensity of vibrational transitions within the optical excitation of PTCDI oligomers (see Supporting Information for a brief discussion).

To examine the viability of either mechanism for the gas-phase dimers requires that excited-state geometries be obtained. To this end, we turn to the lowest energy B3LYP triplet states in **J1** and **J2**, the 1 $^3B_1$ at 989 nm, and the 1 ^3A at 991 nm, respectively. Examination of the NTOs (Figure 7) for both the triplet and optically excited singlet states indicates that they have the same electronic structure, differing only in the total spin. Relative to the ground state, both the B3LYP and BHandH **J1** and **J2** triplet states exhibit contraction of those C−C bonds that lie along the long axis (x) and elongation of the alternate bonds. The excited-state perturbations within each subunit are approximately half that observed in the monomer excited-state geometry, confirming the expected delocalized character of the excitation. However, more relevant is the large predicted nonbonded distortions (e.g., changes in interplanar separation, offset, and rotational orientations) that occur in the excited state. As seen in Table 1, the B3LYP excited-state geometry of **J1** has one subunit rotated by an additional 11° relative to the ground state, while the excited state of **J2** is offset by 0.8 Å along the $-x$ direction. Unlike B3LYP, which found two distinct triplet geometries, the BHandH functional optimized to nearly the same triplet geometry for both **J1** and **J2**. This structure has one subunit rotated by 5° and is offset by 2 Å relative to **J2**. Compared to experiment, the nonbonded excited-state displacements are likely overemphasized because the triplet state does not account for the attractive transition dipole coupling term within the multipole expansion that contributes to the dispersion interaction between chromophoric units. However, our studies and previous studies[37] imply that the potential energy surface along the displacement coordinates is shallow, and thus translational and rotational displacements can be expected in the excited-state conformations of PTCDI oligomers, particularly in solution.

Considering first the displaced harmonic oscillator model for simulating the vibronic spectra of **J2**, we obtained the FC factors and the simulated vibronic spectra as shown Figure 8. The **J2** conformation, which exhibits primarily translational distortion in the excited state, has a B3LYP and BHandH vibronic

(37) Hobza, P.; Selzle, H. L.; Schlag, E. W. *J. Phys. Chem.* **1996**, *100*, 18790.

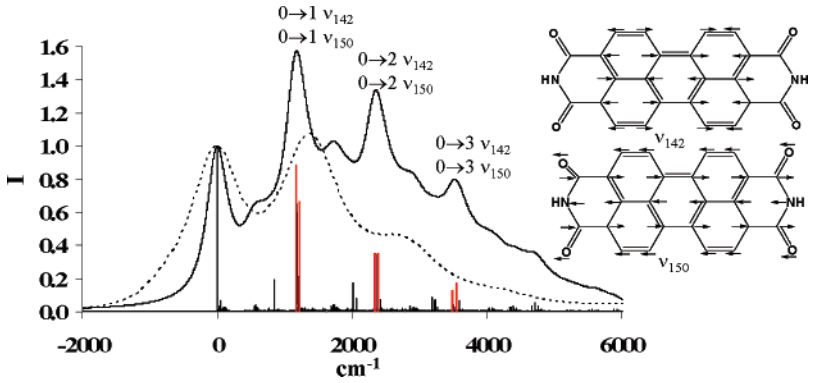

Figure 8. Simulated B3LYP vibronic progression (solid line, sticks) of gas-phase PTCDI dimer **J2**, overlaid with the experimental spectra of ethylene glycol linked PTCDI dimer (dot).[13] Contributing modes are inset and highlighted in red.

spectrum that qualitatively agrees with experiment, including the observed intensity enhancement of the bands past the 0 → 0 transition. In the B3LYP simulation, four peaks are present, separated by ~1200 cm^{-1}. Analysis of the FC factors indicates that transitions within two vibrational modes dominate the spectra: ν_{142} (B, $h\nu$ = 1168 cm^{-1}) and ν_{150} (A, $h\nu$ = 1211 cm^{-1}). These C−C stretches are composed solely of atomic displacements along the long axis of each subunit, which corresponds to the direction of displacement observed in the excited-state structure. In the context of the displaced harmonic oscillator model, ν_{142} and ν_{150} have a large enough displacement that their higher quanta transitions exhibit significant intensity enhancement. This is a particularly relevant result, as enhancement is generally associated with ground-state H-aggregates, not J-type structures. Several other modes have smaller FC contributions to the vibronic spectrum, including those C−C vibrations that couple to the electronic transition within PTCDI monomer. However, the B3LYP 0.8 Å excited-state displacement along the *x*-axis in **J2** causes the FC factors of ν_{142} and ν_{150} to be 2 orders of magnitude larger than the vibrations which overlap well with the geometric changes predicted in the individual subunits. This enhancement is only further enhanced in the BHandH simulation. It is likely that quantitative agreement with experiment would be obtained if the two types of modes had FC factors that were similar in magnitude.

The second mechanism that may contribute to changes in vibronic band intensity is Herzberg−Teller coupling,[16] however, there are several factors that indicate it may not be the dominant factor in gas-phase dimer enhancement. Foremost is the observation that the vibrational modes which exhibit large distortions in the excited state do not correspond to those with large FC factors in the monomer. As a test for the contributions of HT coupling to vibronic band enhancement, we manually displaced a subunit along a vibrational mode that participated in the spectrum in PTCDI monomer and then recalculated the dimer FC factors. No qualitative difference was observed in the simulated spectrum relative to Figure 8. The same conclusions are reached with the BHandH functional.

Unlike the **J2** isomer, the B3LYP excited-state geometry of **J1** is characterized by rotation of one subunit by 11°, which alters both the *x* and *y* subunit atomic coordinates. The BHandH triplet structure is rotated by ~8° relative to the **J1** ground state. From the FC point of view, rotation is a much larger displacement than the pure lateral motion. As such, there is a large amount of overlap between the ground- and excited-state vibrational wave functions, and nearly every vibration has a significant FC factor. In a system of this size, it is impossible to calculate all of the FC factors, and the net result would be a spectrum with a single broadened peak that spans a 4000 cm^{-1} range, devoid of structure. Since this is not observed in the experimental system, excited-state rotation is disregarded as a means for the observed intensity enhancements within the vibronic progression of PTCDI oligomers.

Conclusions

The optical properties of gas-phase perylene tetracarboxylic diimide (PTCDI) and its chromophoric dimer have been examined as a function of conformation to relate the excited-state distributions predicted by exciton theory with that of TDDFT. Using ground- and excited-state geometries, the origin of the dramatic intensity reversal of 0 → 0 and 0 → 1 vibronic bands in the π to π^* transition of PTCDI oligomers has also been determined. Both B3LYP and BHandH functionals have been used, and qualitatively the same conclusions may be drawn from either functional.

For PTCDI monomer, Franck−Condon analysis predicts that four vibrations (and their combination bands) contribute significantly to the normal vibronic progression observed in the electronic spectrum. In the case of the chromophoric dimer, two optimized geometries were obtained, each of the J-type. The excited-state distortions within each subunit of PTCDI dimer were approximately half of that predicted for the monomer, confirming the delocalized character of the lowest energy optical excitation. However, significant nonbonded displacements (translation and rotation of one subunit with respect to the other) were predicted for the excited-state geometries. In the context of a displaced harmonic oscillator model, excited-state translation led to enhancement of the higher quanta transitions of vibrations whose motion was along the translation coordinate. Qualitative agreement was obtained for the structure of the PTCDI dimer optical absorption. Excited-state rotation was eliminated as a possibility for the intensity reversal of the 0 → 0 and 0 → 1 bands. Since HT coupling is known to cause vibronic enhancement in H-aggregates, our results show that J-aggregates can also exhibit enhancement but via nonbonded excited-state distortions, which lead to large FC factors for vibrations whose motion lies along the displacement axis. Finally, a detailed examination of the TDDFT exciton splitting patterns of idealized PTCDI chromophoric dimers indicates that

the energy of the Frenkel transition in these aggregates may not be a good indicator of oligomer conformation.

This study has significant implications for electron−phonon coupling in stacked chromophores and experimental work, where the vibronic intensity reversal is used to diagnose macromolecular folding or self-organization of supramolecular systems.

Acknowledgment. The authors thank Patrik Callis (MSU) for supplying the Bozesuite program and for helpful comments regarding this work. This study was funded in part by startup funds provided by WSU.

Supporting Information Available: Complete ref 24; details regarding the calculation of FC factors and a review of exciton theory, in addition to all Cartesian coordinates, vibrational frequencies, and FC factors. This information is available free of charge via the Internet at http://pubs.acs.org.

JA0687724